ANALYSIS ON HEAT TRANSFER PERFORMANCE SUB-CHANNELS OF SODIUM-COOLED FAST REACTOR FUEL ASSEMBLIES BASED ON ENTRANSY

by

Zenghao DONG, Jianquan LIU [*], Chao HUANG, Xinyi NIU, and Lihan HAI

Shanghai University of Electric Power, Shanghai, China

In this paper, the symmetric heat transfer performance of sodium-cooled fast reactor fuel assemblies was analyzed and studied. The model is analytically optimized based on sub-channel calculations. The deviations of the numerical simulation results from the pre-existing experimental data in the literature are within 10 %, with an average deviation of 2.5 %, which tested the reliability of the model. The calculated results demonstrated that the distribution of the axial power, temperature, and coolant of the reactor core is approximately symmetric M-shape. The reactor core coolant has a monotonic increase in axial distribution with the cladding temperature and the temperature peaks all appear at the reactor core outlet. The individual fuel assemblies' internal temperature is relatively sensitive to the axial power distribution, and there are troughs around the imports and exports. The simulated results showed that the center temperature of the hottest rod reactor core block reached 965.65 K. This paper provides a better guide to understanding the overall heat transfer effect by optimizing the heat transfer model.

Key words: sodium-cooled fast reactor, fuel assembly, sub-channel method, entransy dissipation

INTRODUCTION

As one of the 4th-generation nuclear reactors, the sodium-cooled fast reactor has attracted the attention of many scholars in the world since it was proposed. Compared with the existing reactor types, it has obvious economic and structural advantages [1]. For fast reactors cooled by liquid sodium metal, the study of heat transfer characteristics of reactor core fuel assemblies has always been an indispensable part of the evaluation of the reactor core heat transfer process. In this paper, based on the layout and operating conditions of a theoretically designed single-box fuel assembly of the sodium-cooled fast reactor, the sub-channel analysis program is used to model the heat transfer process of the reactor core and evaluate the preliminary heat transfer performance, to lay a good foundation for the subsequent design optimization of the heat transfer process of sodium-cooled fast reactor fuel assembly. The influence of reactor system parameters, including system pressure, heat flux, and mass flow rate, on the safety and efficiency of reactor operation is particularly critical [2]. Many scholars at home and abroad have analyzed the influence of system parameters on

wall temperature and heat transfer coefficient in the study of reactor core sub-channels. The good agreement between tested reactor data and subchannel model code calculation concerning the reactor demonstrates the reliability of the analysis methodology from a thermal-hydraulic perspective [3, 4]. Most of the existing studies analyze the heat transfer characteristics of the coolant sodium flow process for cladding temperature, heat transfer coefficient, and flow resistance [5].

The equivalent thermal resistance defined based on the dissipation of entransy as a cornerstone is an index to evaluate the overall heat transfer performance of the system. Starting from the comparison of heat conduction and conductive processes, it is applied to multidimensional, unsteady, and complex heat transfer problems with internal heat sources [6]. A new physical quantity corresponding to the energy of a capacitor is introduced, entransy, which has the meaning of *energy* and describes the total capacity of an object to transfer heat. Given that it is 1/2 of the product of temperature and heat capacity, this physical quantity is called entransy [7]. The heat transfer process is an irreversible process in which a certain amount of entransy is dissipated. One of the advantages of the entransy equation is that it can be used to optimize the heat transfer process because the conditions

146

Z. Dong, *et al.*, Analysis on Heat Transfer Performance Sub-Channels of ...
Nuclear Technology & Radiation Protection: Year 2023, Vol. 38, No. 3, pp. 145-154

for its establishment require an equilibrium equation so that we can calculate its value through the entransy dissipation function [8]. The equivalent thermal resistance in multidimensional heat conduction problems is specified based on physical quantities of entransy dissipation, thus allowing the extreme value principle of entransy dissipation of heat conduction optimization to be summarized as the principle of minimum thermal resistance for heat conduction optimization.

The physical meaning of the entransy corresponds to the total amount of heat transfer capacity and the dissipation rate of heat transfer capacity, corresponding to the electrical energy stored in the capacitor. Heat transfer analysis shows that the entransy of an object describes its heat transfer capacity, as the electrical energy in a capacitor describes its charge transfer capacity [9]. The entransy dissipation of substances during heat transfer occurs as a measure of the irreversibility of heat transfer. The introduction of the extreme value principle of entransy dissipation provides a completely different perspective for heat transfer optimization and solves the previous limitations and backwardness of heat assessment by entropy generation and thermal resistance as evaluation indicators [10].

The entransy dissipation of the heat transfer process and the mechanical energy dissipation generated by the fluid transfer process are identical [11]. The extreme value principle of entransy dissipation provides a new theoretical basis for heat transfer optimization, differing from the traditional techniques of enhanced heat transfer processes and the extreme value of entropy generation. Nowadays, the theoretical approaches for enhanced heat transfer are broadly entropy generation analysis method, field synergy principle, and entransy dissipation method [12]. The entransy dissipation method avoids the *entropy production paradox* of the entropy production method and is simpler than the field synergy method. The physical quantity of fire product is obtained by thermoelectric comparison based on similarity in the mode of transfer and is used to define the strength of the heat transfer capability of an object [13]. There are two main ways of optimizing the entransy dissipation method for heat transfer processes: one is to find the best distribution of variables to minimize the heat transfer temperature difference for a given heat flow condition and this phenomenon is the minimum entransy dissipation and the other is to maximize the heat flow transferred for a given temperature difference when the process is expressed as the maximum dissipation of entransy. The combination of these two cases is the extreme value principle of entransy dissipation [14].

The sub-channel program can calculate the temperature and velocity distribution of the fluid at the reactor core scale. However, it still has certain limitations. A lot of research on the sub-channel program is needed to improve the calculation accuracy of the

sub-channel program. In this paper, the sub-channel program has been used to simulate the cooling process of the fuel assembly of the sodium-cooled fast reactor. The thermal-hydraulic analysis of the sub-channel and the study of the entransy dissipation law under the steady state of the reactor has been carried out, aiming to provide a heat transfer evaluation method based on the second law of thermodynamics and focusing on the thermal-hydraulic characteristics of the reactor core, in addition to the existing conventional methods.

NUMERICAL SIMULATION

Mathematical model

This paper is aimed at the sodium-cooled reactor. The boiling point of sodium is very high. Considering the design operating parameters of the concept reactor, it will not reach the boiling state. Therefore, the program uses a single-phase flow model and does not consider two-phase flow and heat transfer [15]. In the processing of turbulent mixing, the equal-mass model is used, that is, the exchange of energy and momentum between subchannels is considered without considering the mass exchange. Since it is the main factor affecting the enthalpy drop of the hot channel, the introduction of this model can improve the accuracy of the solution [16]. This program uses the division method of sub-channels formed by connecting the centerline of the fuel rod, the vertical pipe wall line, and the inner wall of the assembly. The following is the analytical model of the program [17, 18]:

Mass conservation equation can be expressed as

$$ A_i \frac{\partial \rho_i}{\partial t} \quad \frac{\partial m_i}{\partial z} \quad \sum_{j \; i}^{N} w_{ij} \tag{1} $$

where A_i, ρ_i, m_i, are the flow area, the coolant density, and the axial mass flow rate of subchannel i [19], w_{ij} – the horizontal flow, and z – the height of axial control volume.

Energy conservation equation can be expressed as

$$ \rho_i A_i \frac{\partial h_i}{\partial t} \quad \frac{\partial m_i h_i}{\partial z} $$

$$ \sum_{j \; i} w_{ij} h \quad \overline{q_i} \quad \sum_{j \; i} G_D \lambda \frac{s_{ij}}{l_{ij}} (T_i \quad T_j) \tag{2} $$

where h_i is the enthalpy, w_{ij} – the turbulent mass flow rate, h – the turbulent enthalpy, $\overline{q_i}$ – the channel i inline power, G_D – the thermal conductivity factor, λ – the thermal conductivity of material, s_{ij} – the length of the gap between channels i and j, l_{ij} – the turbulence length, and T_i, T_j, are the channel and adjacent channel temperatures.

Axial momentum conservation equation can be expressed as

$$\frac{\partial m_t}{\partial t} \quad \frac{1}{\rho_i A_i}\frac{\partial m_i^2}{\partial z} \quad _j \quad _i \quad w_{ij}U$$

$$A_i\frac{\partial p}{\partial z} \quad \rho_i g A_i\cos\theta \quad \frac{fm_i|m_i|}{2D_e\rho_i A_i} \quad f_T \quad _j \quad _i \quad w_{ij}U \tag{3}$$

where U is the axial velocity, p – the pressure, g – the gravitational acceleration, θ – the angle between the flow and the vertical direction, f – the frictional drag coefficient, D_e – the channel hydraulic diameter, f_T – the turbulent momentum factor, and U – the turbulent cross-mixing transverse flow.

Transverse momentum conservation equation can be expressed as

$$\frac{\partial w_{ij}}{\partial t} \quad \frac{\partial(w_{ij}U)}{\partial x} \quad \frac{s_{ij}}{l_{ij}} \quad _j \quad _i \quad (p_i \quad p_j) \quad \frac{1}{2}K_G\frac{|w_{ij}|w_{ij}}{\rho_i s_{ij}l_{ij}} \tag{4}$$

where p_i, p_j are the adjacent channel pressure, and K_G – the cross-flow resistance coefficient.

Physical model

Fluid physical model

The melting point of sodium at atmospheric pressure is 370.95 K, and the flow characteristics of liquid sodium are close to those of water, but its thermal conductivity is two orders of magnitude higher than that of water, making it extremely capable of conducting heat. The boiling point of sodium at atmospheric pressure is 1156.15 K, which is higher than the design temperature of the fast reactor and ensures its safety, so liquid sodium metal is a very good coolant for the fast reactor. By now, most of the fast reactors in the world have been built using liquid sodium metal as coolant. The physical parameters of sodium used in this study such as density, isobaric specific heat capacity, kinetic viscosity, and thermal conductivity are shown in tab. 1 [20-22]

Convective heat transfer formula

Liquid sodium metal has a lower Prandtl number. Compared with ordinary fluids, liquid metals have high thermal conductivity. In convection heat transfer, molecular heat conduction is the main one. In the process of convection heat transfer, there is a phenomenon of separation of temperature boundary layer and velocity boundary-layer. The heat transfer characteristics are fundamentally different from those of conventional fluids. The Pr 0.007 of liquid sodium indicates that in the convective heat transfer process of liquid metal sodium, the heat conduction process cannot be omitted relative to the momentum heat diffusion transfer process, and it can even play a leading role under individual conditions [23]. This difference will eventually be reflected in the relationship of the dimensionless Nu for heat transfer. The Dittus-Boelter relationship, which ignores the thermal conductivity of molecules, is only suitable for water, not for liquid metals with low Prandtl numbers. The convective heat transfer relationship for the process of liquid metal sodium cooling reactor core can be expressed as [24]

$$\text{Nu} \quad 4.0 \quad 0.16\left(\frac{P}{D}\right)^{5.0} \quad 0.33\left(\frac{P}{D}\right)^{3.8}\left(\frac{\text{Pe}}{100}\right)^{0.86} \tag{5}$$

Scope of application of this formula: $1.15 \quad P/D \quad 1.30, 10 \quad \text{Pe} \quad 5000$. In eq. 5, P is the rod spacing, D – the outer diameter of the rod, and Pe is the Peclet number, which is a dimensionless value equal to the product of the Reynolds number and the Prandtl number [25]. When calculating the Reynolds number in this simulation process, the characteristic length d is taken as the equivalent diameter, and the characteristic velocity is taken as the flow rate of the reactor core coolant.

Friction pressure drop formula

Novendstern proposed a semi-empirical model for hexagonal wire-wound fuel rod assemblies. In this model, the winding is represented by an additional coefficient of friction. The pressure drop for a smooth tube is first calculated using the Blasius relation. The winding problem is then explained by introducing a multiplier M [26], *i. e.*

$$f \quad M\frac{0.3164}{\text{Re}} \tag{6}$$

Table 1. Liquid sodium physical property relationship

Parameter	Unit	Value/Formula
Melting point	K	$T_M = 370.95$
Boiling point	K	$T_B = 1156.15$
Enthalpy of liquid	Jkg^{-1}	$h_s = -6.7511\ 10^4 + 1630.22T \quad 0.41674T^2 + 1.54279\ 10^{-4}\ T^3$
Density	kgm^{-3}	$\rho = 10011.6 \quad 0.22051T \quad 1.92243\ 10^{-5}\ T^2 + 5.63769\ 10^{-9}\ T^3$
Isobaric specific heat	J(kgK)^{-1}	$C_p = 1630.22 \quad 0.83354T + 4.62838\ 10^{-4}\ T^2$
Kinetic viscosity	Nsm^{-2}	$\mu = 10^{-2.4892} + 220.65\ T^{-1} \quad 0.4925\ \log_m^T$
Thermal conductivity	W(mK)^{-1}	$\lambda = 109.7 \quad 6.4499\ 10^{-2}\ T - 1.1728\ 10^{-5}\ T^2$

148

Z. Dong, *et al.*, Analysis on Heat Transfer Performance Sub-Channels of ...
Nuclear Technology & Radiation Protection: Year 2023, Vol. 38, No. 3, pp. 145-154

where *M* is a function of flow parameters and structural parameters, which can be expressed as

$$M = \left[\frac{1.034}{(P/D)^{0.124}} + \frac{29.7(P/D)^{6.94} \, Re^{0.086}}{(H/D)^{2.239}} \right]^{0.885} \quad (7)$$

The applicable range of the Novendstern model is $2600 < Re < 200000$, $1.05 < P/D < 1.42$, $8 < H/D < 96$.

Subchannel model

According to the system parameters of the fuel assembly in sodium-cooled fast reactors, the operating pressure of the reactor is 0.43 MPa, the inlet temperature of the sodium coolant from the bottom of the reactor core is 633.15 K, and the inlet flow rate of the sodium coolant takes a uniform distribution. China Experimental Fast Reactor (CEFR) adopts a hexagonal type for fuel assembly. The model is divided into an inlet section and an active section, assuming equal inlet pressures in each channel. The power of each fuel rod of the assembly used in this paper is equal and uniformly distributed. The subchannels can be divided into internal channels, side channels, and corner channels according to their positions and shapes. The basic parameters of the fuel assembly are given in tab. 2.

There are 61 fuel rods in a single fuel assembly, arranged in a triangular pattern and positioned using wire wrap. Each of the 61 fuel rods was numbered counterclockwise in a circular fashion from the inside to the outside as shown in fig. 1. At the same time, the coolant channels in the fuel assembly are divided into different subchannels, which are classified as inner channel, corner channel, and side channel according to the location of the flow channels, and a total of 126 subchannels are classified. Among all subchannels,

Table 2. Basic parameters of the fuel assembly

Parameter	Unit	Value/description
Full length	m	2.592
Number of pins		61
Center distance	m	$7 \cdot 10^{-3}$
Full length of cladding	m	1.313
The outer diameter of the cladding	m	$6 \cdot 10^{-3}$
The inner diameter of the cladding	m	$5.4 \cdot 10^{-3}$
Coolant flow rate	ms^{-1}	<5
Cladding material		CN-1515
Maximum temperature of cladding	K	943.15
Inlet and outlet temperature	K	633.15/803.15
Maximum line power density	kWm^{-1}	4.10

there are 6 corner channels, 24 side channels, and 96 inner channels.

Entransy dissipation analysis model

Entransy dissipation in the heat transfer process

Under the condition of the given parameters, according to the obtained operating state, using the definition formula of entransy flow, the entransy flow caused by the heat transfer of the fuel rod can be obtained as

$$E_l = CqT_c \pi D \Delta l \quad (8)$$

where *C* is the thermal cycle coefficient, *q* – the heat flux density between the cladding and the coolant, T_c – the cladding temperature, and Δl – the axial pitch.

Since the entransy dissipation is a state quantity, the entransy dissipation change of the sodium fluid is calculated according to the flow parameters of the so-
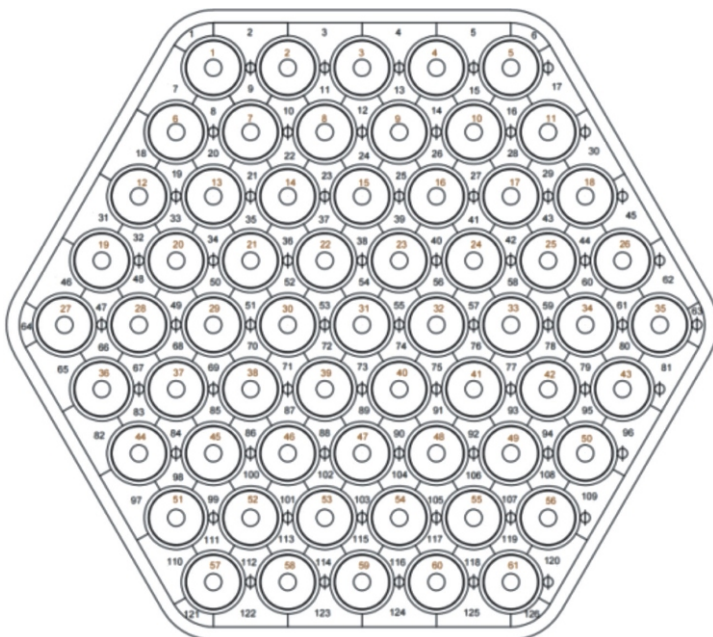
Figure 1. Sub-channel division of fuel assembly

Z. Dong, *et al.*, Analysis on Heat Transfer Performance Sub-Channels of ...
Nuclear Technology & Radiation Protection: Year 2023, Vol. 38, No. 3, pp. 145-154

149

Table 3. Comparison of deviations of subchannel program results with experimental

Term of comparison	Subchannel program temperature [K]	Experimental temperature [K]	Misalignment
Subchannel maximum sodium temperature	840.65	845.05	0.52 %
Average subchannel outlet temperature	800.55	811.45	1 %
Subchannel maximum sodium temperature rise	480.65	485.05	0.91 %
Peak shell temperature	853.25	885.95	3.69 %
Peak fuel temperature	965.65	990.35	2.50 %

dium fluid, and the entransy dissipation increment of the sodium fluid can be expressed as

$$E_2 = \frac{1}{2} m l U \, {}^1 C_p T_f^2 \qquad (9)$$

where m is the axial mass flux, l – the turbulent length, U – the axial velocity, C_p – the constant-pressure specific heat, and T_f – the coolant temperature.

Entransy dissipation in the flow process

Assuming that the flow of the sodium in the channels is caused by the pressure difference between the outlet and the inlet, and the flow is adiabatic in a steady state, ignoring the effect of the enthalpy change for the entransy, it can be obtained as

$$\mathrm{d}e - \frac{T\mathrm{d}p}{\rho} = 0 \qquad (10)$$

where ρ is the fluid density, p – the pressure, and e – the specific entransy, that is, the entransy per unit mass of fluid.

In the subchannels, only the entransy dissipation of the flow process is considered, the above formula is integrated, and the average temperature of the fluid is used to approximate the temperature of sodium, then the entransy dissipation caused by the fluid resistance can be expressed as

$$E_3 = \frac{T_{\text{in}} - T_{\text{out}}}{2} \frac{m}{\rho} P \qquad (11)$$

RESULTS AND DISCUSSION

Comparison of deviation of simulation results

The STAC subchannel program was used to calculate the thermal-hydraulic parameters of the CEFR fuel elements under steady state conditions and compare them with the experimental control values in the *China Experimental Fast Reactor Project One-Circuit Main Cooling System Manual* and the safety analysis report. Table 3 lists the comparison and deviation statistics between the arithmetic calculation results of the subchannel program and the experimental control values.

As can be seen from tab. 3, the data of subchannel maximum sodium temperature, subchannel outlet average temperature, and subchannel maximum sodium temperature rise calculated by the STAC program have a small deviation from the experimental control value,

which is less than 2.5 %, and the calculated results of peak shell temperature and peak fuel temperature have a slightly larger deviation from the experimental control value, which is less than 10 %. The comparison results show that the deviation of the arithmetic results from the experimental control values is less than 10 %, and the average deviation of each result is close to 2.5 %. The modeling of the STAC subchannel program in the set steady state condition is basically correct, and it can be used for the analytical study in the subsequent chapters in combination with entransy dissipation theory.

Thermal parameters analysis of the subchannels

Power distribution

Figure 2 shows the axial power distribution of reactor core, which is approximately a cosine function distribution, the power peak appears near the axial height of 0.4 m, and the crest factor is about 1.234. Affected by the thermal insulation layer, the power at the upper and lower ends of reactor core increases, resulting in different power valleys in the 0-0.1 m interval and the 0.7-0.8 m interval.

Axial distribution of coolant temperature

Figure 3 shows the axial distribution of coolant in 12 groups of channels in the fuel assembly. It can be observed from the figure that the coolant temperature
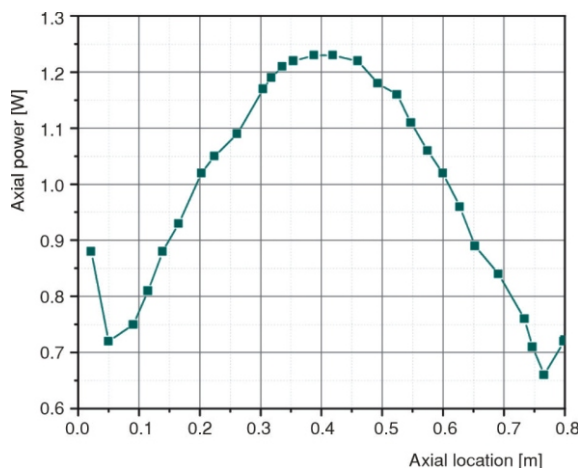
Figure 2. Power distribution

150

Z. Dong, *et al.*, Analysis on Heat Transfer Performance Sub-Channels of ...
Nuclear Technology & Radiation Protection: Year 2023, Vol. 38, No. 3, pp. 145-154
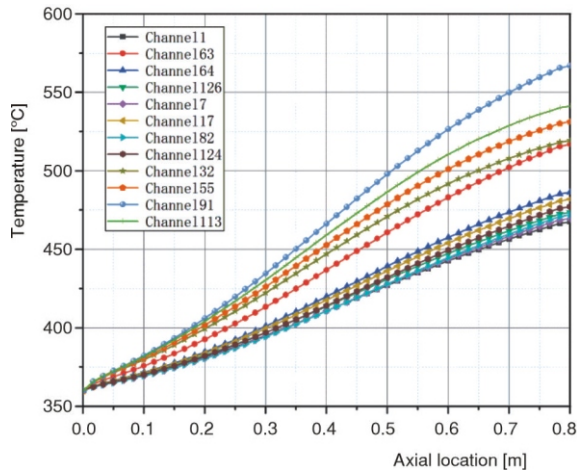
Figure 3. Axial distribution of coolant temperature

in the channels increases continuously with the axial height and the maximum temperature value appears at the exit of the channels. The exit temperature of the edge 1 channel and 126 channel assembly is slightly lower than the other channels, which is due to the large difference in the circulation area of the different flow channels within the assembly. The larger equivalent diameter and the larger flow area of the subchannels will lead to a better cooling effect and lower temperature of the subchannels.

Axial distribution of cladding temperature

Figure 4 shows the axial distribution of the outer surface temperature of the cladding for different fuel rods. It can be observed from the figure that the increase of the cladding temperature is relatively flat in the interval of 0-0.1 m due to the change of axial power distribution and coolant flow, in the interval of 0.1-0.8 m, the increase of the cladding temperature is sharp and then flat due to the change of axial power distribution and reaches the maxi-

mum value at the exit. The temperature of the cladding of fuel rods 57 and 61 is significantly lower than that of fuel rods 42 and 53 and is smaller than that of other fuel rods. The reason for this is that the better the cooling effect is, the lower the fuel rod casing temperature is, and the casing temperature in the other channels also shows a large difference depending on the channel type.
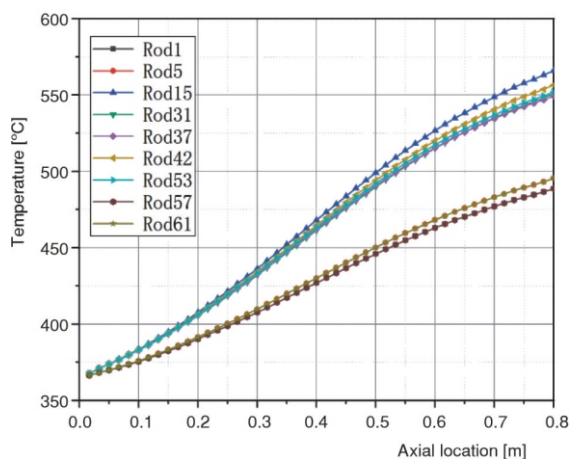
Axial temperature distribution of the hottest rod

Figure 5 shows the axial temperature distribution of the hottest rod in fuel assembly. The axial temperature distribution of the hottest rod includes the center temperature of fuel, the outer surface temperature of fuel, the inner surface temperature of the cladding, the outer surface temperature of the cladding, and the temperature of the coolant. The peak temperature of fuel pellet is 965.61 K. The maximum temperature difference between the center and outer surface of the fuel rod occurs at 0.45-0.55 m with a value of 349.02 K. The impact of thermal stress fatigue loss on the structural strength of the fuel pellet needs to be focused on here. The temperature at the top and bottom of reactor core increases slightly due to the increased neutron moderation which leads to increased energy release from the fission reaction and increased power at the endpoints, resulting in slightly higher temperatures at both ends of the fuel rod. The peak temperature of the cladding is 853.18 K. The difference in the fuel rod temperature is large because of the inadequate heat transfer caused by the large thermal resistance of the air gap between the fuel rod and the cladding. From fig. 5, it can be seen that the increase of rod temperature at both ends has obvious feedback on the cladding temperature, showing the same trend of change. The temperature of the coolant increases monotonically with the axial height, and the maximum temperature value appears at the channel exit, with the value of 840.68 K.

Figure 4. Axial distribution of cladding temperature
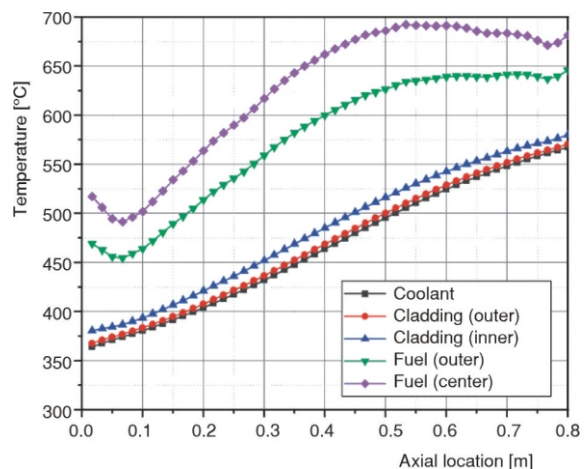
Figure 5. Axial temperature distribution of the hottest rod

Z. Dong, *et al*., Analysis on Heat Transfer Performance Sub-Channels of ...
Nuclear Technology & Radiation Protection: Year 2023, Vol. 38, No. 3, pp. 145-154

151

Entransy analysis of subchannels

Axial distribution of fractional entransy dissipation

Figure 6 shows the axial distribution of fractional entransy dissipation for different types of subchannels. Three typical channels are selected in this paper, Channel 1 is the corner channel, Channel 55 is the inner channel, and Channel 124 is the side channel. The fractional entransy dissipation of each channel generally shows the same trend, which decreases in a linear trend in the range of 0-0.8 m. The difference in the entransy dissipation of flow fraction is analyzed due to the dominant influence of the flow area and mass flow rate of the side Channel 124. The mass-flow rate of the angular channel is slightly faster than that of the inner channel, but the effect is not as fierce as the temperature pattern of the inner channel.

Axial entransy distribution of coolant flow process

As shown in fig. 7, the axial entransy distribution of coolant flow process for different types of subchannels. The overall coolant entransy flow in each channel showed an upward trend, and the coolant entransy flow in the side channel was larger. The entransy flow in Channel 124 is significantly higher than in other channels. The reason for this condition is that the flow area and mass-flow of the side channel are larger than those of the corner channel and the inner channel, the coolant fluid temperature and mass-flow of the corner channel are the smallest, but the mass-flow rate is higher than that of the inner channel.

Axial entransy distribution of heat transfer process

As shown in fig. 8, the axial entransy distribution of heat transfer process of different types of
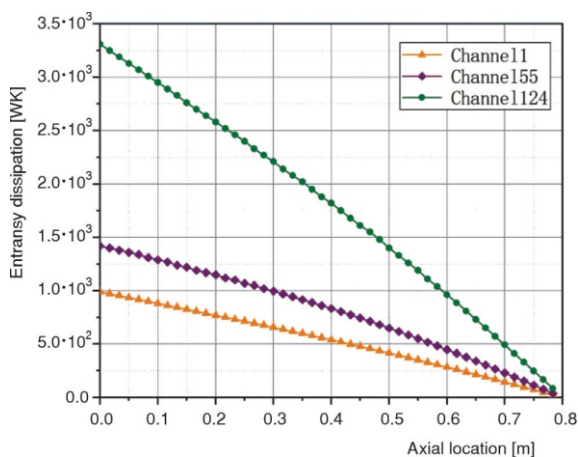
Figure 6. Axial distribution of fractional entransy dissipation
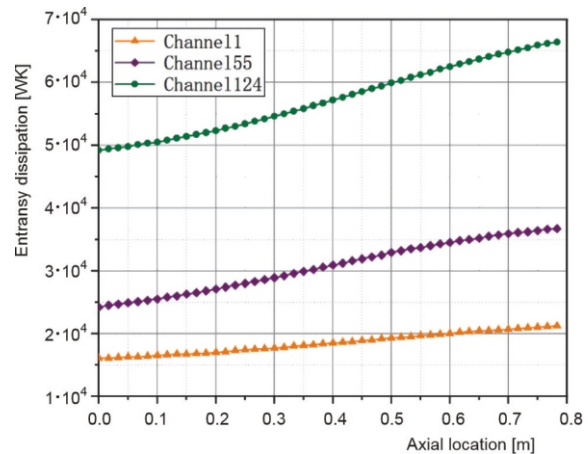
Figure 7. Axial entransy distribution of coolant flow process
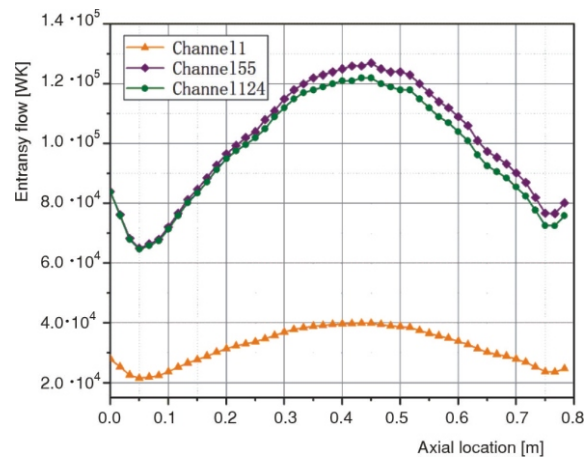
Figure 8. Axial entransy distribution of heat transfer process

subchannels. The entransy flow shows a similar distribution to the power due to the axial power distribution variation and coolant flow. It can be seen from the figure that the distribution of entransy flow in Channel 1 is generally lower than that in Channel 55 and Channel 124. The reason is that the heated perimeter of the corner channel is smaller than that of the side channel and the inner channel, resulting in a small entransy flow. The higher entransy of the side channel is due to the poorer cooling effect of the inner channel than that of the side channel.

Axial entransy dissipation distribution of subchannels

As shown in fig. 9, the axial entransy dissipation distribution of subchannels in different types of fuel assembly. It can be seen from the figure that the overall trend is greatly affected by the power distribution, and the trend is relatively uniform. The entransy dissipation of corner Channel 1 is the smallest and the trend is the most gentle, indicating that the entransy dissipa-

152

Z. Dong, *et al.*, Analysis on Heat Transfer Performance Sub-Channels of ...
Nuclear Technology & Radiation Protection: Year 2023, Vol. 38, No. 3, pp. 145-154
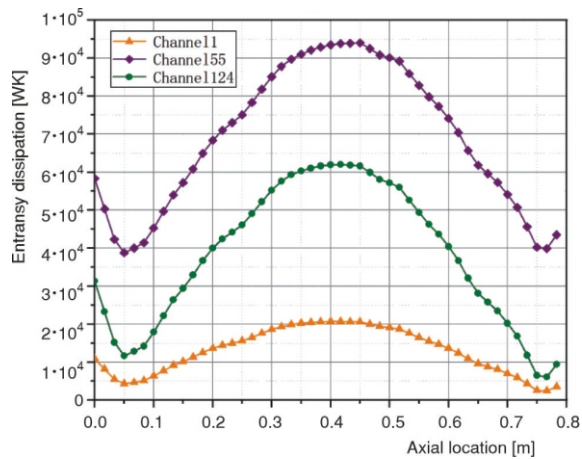
Figure 9. Axial entransy dissipation distribution of subchannels

tion in the heat transfer process of this channel is least affected by the power. Under the same heated perimeter conditions, the entransy dissipation of the side Channel 124 is significantly smaller than that of the inner Channel 55, the reason is that the wet perimeter of the side channel is larger than that of the inner channel, resulting in negative feedback.

Axial distribution of the entransy dissipation rate

As shown in fig. 10, the axial distribution of the entransy dissipation rate for different types of subchannels of the fuel assembly. It can be seen that the entransy dissipation rate of the inner Channel 55 is significantly higher than that of the side channel and the corner channel. However, the trend of the entransy dissipation rate of the side channel and the corner channel is basically the same, and the changing trend of the inner channel is more moderate. The reason for
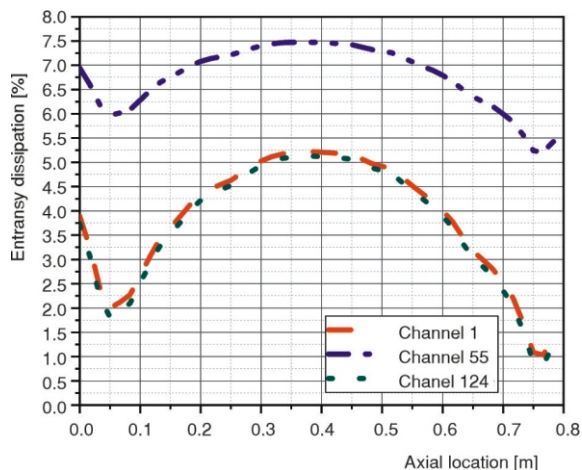
Figure 10. Axial distribution of the entransy dissipation rate

this condition is that the complex structure and lateral mixing of the inner channel are taking effect. The inner channel has a larger heated perimeter and a smaller wetted perimeter, which leads to a larger entransy flow of heat transfer process and a smaller entransy flow of flow process, so the entransy dissipation rate is larger than that of other channels. However, the inner channel dissipation rate is least affected by the power. The entransy dissipation of the side channel is larger, but the dissipation rate is the smallest. The reason for this condition is the negative feedback generated by the large mass flow rate.

CONCLUSIONS

The analytical model of sub-channel is established with the sub-channel program STAC as a tool and CEFR as a research object, and its steady-state thermal parameters and the inlet dissipation law of sub-channel are analyzed. The results show that:

Based on the subchannel analysis program STAC, CEFR is chosen as the model for core symmetry subchannel analysis, and the subchannel steady-state thermal parameters and subchannel entransy dissipation law are analyzed. The results show that the plutonium enrichment of the component determines the approximate symmetric cosine function distribution of reactor core axial power, which further affects the component temperature and coolant flow. Therefore, the distribution of axial power, temperature, and coolant flow is approximately symmetric *M*-shaped.

The reactor core coolant and casing temperatures increase monotonically in the axial direction, and the temperature peaks are found at reactor core outlet. The internal temperature of the individual components is sensitive to the axial power distribution, and there are valleys near the inlet and outlet. In addition, the larger the equivalent diameter of the circulation channel, the larger the circulation area and the better the cooling effect. The final calculation shows that the center temperature of the hottest rod core reaches 965.65 K, which is lower than the melting point of the nitride fuel. The validation shows that the results of the STAC thermal analysis program are in good agreement with the literature data and can be applied to the thermal hydraulic analysis of the sodium-cooled fast reactor core.

The entransy dissipation of the subchannels is represented by the comprehensive influence trend of power distribution, mass-flow rate, and channel structure. The corner channel is least affected by power and the entransy dissipation is the least. The inner channel is affected by the mass-flow rate and channel structure resulting in the largest entransy dissipation. Due to the complex structure and lateral

Z. Dong, *et al.*, Analysis on Heat Transfer Performance Sub-Channels of ...
Nuclear Technology & Radiation Protection: Year 2023, Vol. 38, No. 3, pp. 145-154

153

mixing of the inner channel, the entransy dissipation rate is larger than that of the edge channel. Due to the influence of the mass-flow rate, the side channel shows the most excellent heat transfer performance with a low entransy dissipation rate corresponding to a larger entransy dissipation.

ACKNOWLEDGMENT

AUTHORS' CONTRIBUTIONS

Z. Dong: conceptualization, methodology, software, writing-review and editing. J. Liu: supervision. C. Huang: validation, writing-original draft preparation; L. Hai and X. Niu: data curation.

Nomenclature

A	Area [m^2]
C	Coefficient of heated perimeter
C_p	Constant-pressure specific heat [$kJkg^{-1}K^{-1}$]
D_e	Hydraulic diameter [m]
e	Specific entransy [$WKkg^{-1}$]
E	Entransy [WK]
G_D	Thermal conductivity factor [$Wm^{-1}K^{-1}$]
f	Frictional drag coefficient
h	Specific enthalpy [Jkg^{-1}]
K_G	Coefficient of local resistance
l	Turbulent length [m]
m	Axial mass flux [kgs^{-1}]
M	Additional coefficient of friction
Nu	Nusselt number ($= hl\lambda^{-1}$)
p	Pressure [Pa]
Pe	Peclet number
Pr	Prandtl number ($= C_p\mu\lambda^{-1}$)
$\underline{q}$	Heat flux [kWm^{-2}]
q_i	Channel i inline power [Wm^{-1}]
Re	Reynolds number ($= UDn^{-1}$)
s	Length of the gap between channels [m]
t	Time [s]
T	Temperature [K]
U	Axial velocity [ms^{-1}]
w	Transverse mass flux per unit length [$kgs^{-1}m^{-1}$]
z	Axial height [m]

Greek symbols

ρ	Density [kgm^{-3}]
θ	Angle between flow and vertical direction [°]
λ	Thermal conductivity [$Wm^{-1}K^{-1}$]

Subscripts

c	Cladding
f	Sodium fluid
i	Volume in axial direction
j	Layer in radial direction

REFERENCES

[1] Yang, H. Y., International Forum on Generation IV Nuclear Energy Systems (GIF) Progress in the development of Sodium-Cooled Fast Reactors, (in Chinese), *Annual Report of China Institute of Atomic Energy,* (2009), 1, pp. 4-5

[2] Gao, X. Z., Ren, L. X., Numerical Simulation Study on Thermal Hydraulics of Lead-Bismuth Fast Reactor Fuel Assembly, (in Chinese), *Technology Innovation and Application,* (2019), 22, p. 4

[3] Hutli, E., Kridan, R.,Thermal-Hydraulic Analysis of Light Water Reactors Under Different Steady-State Operating Conditions, Part 1: Boiling Water Reactor, *Nucl Technol Radiat, 37* (2022), 4, pp. 259-275

[4] Hutli, E., Kridan, R.,Thermal-Hydraulic Analysis of Light Water Reactors Under Different Steady-State Operating Conditions, Part 2: Pressurized Water Reactor, *Nucl Technol Radiat, 37* (2022), 4, pp. 276-288

[5] Zhang S. M., Zhang D. H., Development and Verification of Sub-Channel Analysis Code for Solid Fuel Core of Sodium Cooling Fast Reactor, (in Chinese), *Atomic Energy Science and Technology, 052* (2018), 002, pp. 320-325

[6] Cheng, X. G., Entransy and its Application in Heat Transfer Optimization, (in Chinese), Ph. D. Thesis, Tsinghua University, Beijing, China, 2004

[7] Guo, Z. Y., *et al.*, Entransy-A Physical Quantity Describing Heat Transfer Ability, *International Journal of Heat and Mass Transfer, 50* (2007), 13-14, pp. 2545-2556

[8] Liu, X. B., Entransy Analysis of Thermal Performance of Heat Exchanger and Cooling Channel Network, (in Chinese), Ph. D. Thesis, Tsinghua University, Beijing, China, 2009

[9] Cheng, X., *et al.*, Analyses of Entransy Dissipation, Entropy Generation and Entransy-Dissipation-Based Thermal Resistance on Heat Exchanger Optimization, *Applied Thermal Engineering, 38* (2012), pp. 31-39

[10] Chen, Q., *et al.*, Entransy Theory for the Optimization of Heat Transfer – A Review and Update, *International Journal of Heat and Mass Transfer, 63* (2013), Aug, pp. 65-81

[11] Li, Z. X., Guo, Z. Y., Field Synergy Theory for Convective Heat Transfer Optimization (in Chinese), Science Press, 2010

[12] Chen, X., *et al.*, Entropy and Entransy in Convective Heat Transfer Optimization: A Review and Perspective, *International Journal of Heat and Mass Transfer, 137* (2019), July, pp. 1191-1220

[13] Han, G. Z., *et al.*, Similarities Between Thermal Conductivity and Elastic Systems and Electrical Conductivity, *Academic Conference on Heat and Mass Transfer of Chinese Society of Engineering Thermophysics, 26* (2005), 6, p. 3

[14] Han, G. Z., Guo, Z. Y., The Mechanism of Thermal Conductivity Loss and Its Mathematical Expression (in Chinese), *Proceedings,* CSEE, 27, 2007, 17, p. 5

[15] Wang, X. K., *et al.*, Development of System Code FR-Sdaso for Sodium Cooled Fast Reactor (in Chinese), *Atomic Energy Science and Technology, 54* (2020), 11, p. 9

154

Z. Dong, *et al.*, Analysis on Heat Transfer Performance Sub-Channels of ...
Nuclear Technology & Radiation Protection: Year 2023, Vol. 38, No. 3, pp. 145-154

[16] Moorthi, A., *et al.*, A Review of Sub-Channel Thermal Hydraulic Codes for Nuclear Reactor Core and Future Directions, *Nuclear Engineering and Design, 332* (2018), June, pp. 329-344

[17] Sha, W. T., *et al.*, Boundary-Value Thermal-Hydraulic Analysis of a Reactor Fuel Rod Bundle, *Nuclear Science and Engineering, 59* (2017), 2, pp. 140-160

[18] Lin, C., *et al.*, Preliminary Development of Sub-Channel Code for the Natural Convection Assembly of Sodium Cooled Fast Reactor (in Chinese), *Atomic Energy Science and Technology, 55* (2021), 3, p. 9

[19] Yue, N., *et al.*, The Development and Validation of the Inter-Wrapper Flow Model in Sodium-Cooled Fast Reactors, *Progress in Nuclear Energy, 108* (2018), Sept., pp. 54-65

[20] Xu, Y. J., Thermodynamics in Fast Reactor (in Chinese), Book. Atomic Energy Press, 2011

[21] Shan, J. Q., Qiu H. Z., Research on the Derivation of the Partial Derivative Formula of Sodium Physical Properties for Safety Analysis (in Chinese), *Nuclear Power Engineering, 18* (1997), 3, pp. 238-243

[22] Qiu, R. S., Sodium Technology and Liquid Metal Sodium Circuits (in Chinese), Book, Science Press, 1987

[23] Lyu, K. F., Thermal-Hydraulic Behavior of Liquid Lead-Bismuth Alloy in a Wire-Wound Rod Bundle Assembly (in Chinese), Ph. D. thesis, University of Science and Technology of China, Anhui, China, 2016

[24] Seo, H., *et al.*, Subchannel Analysis of a Small Ultra-Long Cycle Fast Reactor Core, *Nuclear Engineering and Design, 270* (2014), Apr, pp. 389-395

[25] Wang, S., Development of Sub-Channel Analysis Code for Lead-Cooled Fast Reactor Subassembly (in Chinese), Ph. D. Thesis, North China Electric Power University, Beijing, China, 2017

[26] Peng, J., *et al.*, Analysis on the Sub-Channel Program in Sodium-Cooled Fast Reactor (in Chinese), *Proceedings*, 16th National Conference on Reactor Thermodynamic Fluids, 2019, pp. 1463-1475

Ценгхао ДУНГ, Ђенђуен ЉУ, Чао ХУАНГ, Синји ЊУ, Лихан ХАЈ

АНАЛИЗА ПЕРФОРМАНСЕ ПРЕНОСА ТОПЛОТЕ ПОТКАНАЛА ГОРИВНИХ СКЛОПОВА БРЗИХ РЕАКТОРА ХЛАЂЕНИХ НАТРИЈУМОМ НА ОСНОВУ ЕНЕРГИЈА КОНДЕНЗАТОРА

У овом раду анализиране су и истражене перформансе симетричног преноса топлоте горивних склопова брзог реактора хлађених натријумом и модел је аналитички оптимизован на основу прорачуна потканала. Одступања резултата нумеричке симулације од већ постојећих експерименталних података у литератури у границама су од 10 %, са просечним одступањем од 2.5 %, чиме је тестирана поузданост модела. Израчунате вредности показале су да су расподеле аксијалне снаге, температуре и расхладне течности језгра реактора приближно симетричних М-облика. Расхладна течност језгра реактора има монотоно повећање аксијалне расподеле са температуром омотача и температурним врховим на излазу из језгра реактора. Унутрашња температура појединачних горивних склопова је релативно осетљива на аксијалну расподелу снаге, а око улаза и излаза постоје падови. Симулирани резултати показали су да је температура у центру најтоплијег блока језгра реактора са горивном шипком достигла 965.65 K. Овај рад оптимизацијом модела преноса топлоте пружа боље увиде у разумевање укупног ефекта преноса топлоте.

Кључне речи: брзи реактор хлађен натријумом, горивни склоп, субканална метода, дисипација енергије кондензатора